Human Molecular Genetics, 2024, Vol. 33, 12, 1090–1104
https://doi.org/10.1093/hmg/ddae044
Advance access publication date 26 March 2024
Original Article

Functional analysis of cell lines derived from SMAD3-related Loeys-Dietz syndrome patients provides insights into genotype-phenotype relation

Nathalie P. de Wagenaar[1,2,†], Lisa M. van den Bersselaar[3,†], Hanny J. H. M. Odijk[1], Sanne J. M. Stefens[1], Dieter P. Reinhardt[4,5], Jolien W. Roos-Hesselink[2], Roland Kanaar[1], Judith M. A. Verhagen[3], Hennie T. Brüggenwirth[3], Ingrid M. B. H. van de Laar[3,*], Ingrid van der Pluijm[1,6,*], Jeroen Essers[1,6,7,*]

[1]Department of Molecular Genetics, Oncode Institute, Erasmus MC, University Medical Center Rotterdam, Dr. Molewaterplein 40, 3015 GD, Rotterdam, The Netherlands
[2]Department of Cardiology and European Reference Network for Rare Multisystemic Vascular Disease (VASCERN), HTAD Rare Disease Working Group, Erasmus MC, University Medical Center Rotterdam, Dr. Molewaterplein 40, 3015 GD, Rotterdam, The Netherlands
[3]Department of Clinical Genetics and European Reference Network for Rare Multisystemic Vascular Disease (VASCERN), HTAD Rare Disease Working Group, Erasmus MC, University Medical Center Rotterdam, Dr. Molewaterplein 40, 3015 GD, Rotterdam, The Netherlands
[4]Faculty of Medicine and Health Sciences, McGill University, 3640 University Street, Montreal, QC H3A 0C7, Canada
[5]Faculty of Dental Medicine and Oral Health Sciences, McGill University, 3640 University Street, Montreal, QC H3A 0C7, Canada
[6]Department of Vascular Surgery, Cardiovascular Institute, Erasmus MC, University Medical Center Rotterdam, Dr. Molewaterplein 40, 3015 GD, Rotterdam, The Netherlands
[7]Department of Radiotherapy, Erasmus MC, University Medical Center Rotterdam, Dr. Molewaterplein 40, 3015 GD, Rotterdam, The Netherlands
*Corresponding authors. Ingrid M.B.H. van de Laar, Department of Clinical Genetics, Erasmus University Medical Center, P.O. Box 2040, 3000 CA Rotterdam, The Netherlands. E-mail: i.vandelaar@erasmusmc.nl; Ingrid van der Pluijm, Erasmus University Medical Center Rotterdam, Room Ee702b, Wytemaweg 80, 3015 CN Rotterdam, The Netherlands. E-mail: i.vanderpluijm@erasmusmc.nl and Jeroen Essers, Erasmus University Medical Center Rotterdam, Room Ee702b, Wytemaweg 80, 3015 CN Rotterdam, The Netherlands. E-mail: j.essers@erasmusmc.nl

†These authors share first authorship

Abstract

Rationale: Pathogenic (P)/likely pathogenic (LP) *SMAD3* variants cause Loeys-Dietz syndrome type 3 (LDS3), which is characterized by arterial aneurysms, dissections and tortuosity throughout the vascular system combined with osteoarthritis. **Objectives**: Investigate the impact of P/LP *SMAD3* variants with functional tests on patient-derived fibroblasts and vascular smooth muscle cells (VSMCs), to optimize interpretation of *SMAD3* variants. **Methods**: A retrospective analysis on clinical data from individuals with a P/LP *SMAD3* variant and functional analyses on *SMAD3* patient-derived VSMCs and *SMAD3* patient-derived fibroblasts, differentiated into myofibroblasts. **Results**: Individuals with dominant negative (DN) *SMAD3* variant in the MH2 domain exhibited more major events (66.7% vs. 44.0%, $P = 0.054$), occurring at a younger age compared to those with haploinsufficient (HI) variants. The age at first major event was 35.0 years [IQR 29.0–47.0] in individuals with DN variants in MH2, compared to 46.0 years [IQR 40.0–54.0] in those with HI variants ($P = 0.065$). Fibroblasts carrying DN *SMAD3* variants displayed reduced differentiation potential, contrasting with increased differentiation potential in HI *SMAD3* variant fibroblasts. HI *SMAD3* variant VSMCs showed elevated SMA expression and altered expression of alternative MYH11 isoforms. DN *SMAD3* variant myofibroblasts demonstrated reduced extracellular matrix formation compared to control cell lines. **Conclusion**: Distinguishing between P/LP HI and DN *SMAD3* variants can be achieved by assessing differentiation potential, and SMA and MYH11 expression. The differences between DN and HI *SMAD3* variant fibroblasts and VSMCs potentially contribute to the differences in disease manifestation. Notably, myofibroblast differentiation seems a suitable alternative in vitro test system compared to VSMCs.

Keywords: SMAD3; Loeys-Dietz syndrome; functional assay; aneurysmsosteoarthritis syndrome

Introduction

An aortic aneurysm is a local widening of the aorta [1]. Increased aortic diameter is directly associated with an increased risk of aortic dissection or rupture, a life-threatening event [2]. Several genes are associated with aortic aneurysm formation, including genes affecting the TGF-β pathway, the extracellular matrix (ECM), and smooth muscle cell contraction [3].

Genes involved in the TGF-β signaling pathway related to aneurysm formation include *TGFBR1* (LDS1), *TGFBR2* (LDS2), *SMAD3* (LDS3), *TGFB2* (LDS4), *TGFB3* (LDS5), *SMAD2* (LDS6), *SMAD4* (juvenile polyposis/hereditary hemorrhagic telangiectasia), *SMAD6* (bicuspid aortic valve/thoracic aortic aneurysm) and *SKI* (Shprintzen-Goldberg syndrome) [4–14]. *SMAD3* is a signal transducer in the canonical TGF-β pathway. Upon activation by binding of TGF-β, the TGF-β receptor complex activates SMAD3

Received: February 1, 2024. **Revised:** February 23, 2024. **Accepted:** March 6, 2024

and SMAD2 proteins (receptor-regulated Smads; R-SMADs) by phosphorylation. Once phosphorylated, the R-SMADs can form a protein complex with SMAD4 (co-SMAD). Those complexes then transfer to the nucleus where they interact with promotors/co-factors to regulate the transcription of downstream genes, including genes involved in ECM turnover, apoptosis and cellular proliferation, differentiation, motility and adhesion [15–22].

The SMAD3 protein consists of two functional domains separated by a linker region; the N-terminal domain Mad Homology 1 (MH1) and C-terminal domain Mad Homology 2 (MH2). MH1 enables DNA binding and MH2 mediates protein-protein interaction and SMAD-dependent downstream transcription [23]. No mutational hotspots are identified in *SMAD3*, but the majority of the pathogenic/likely pathogenic (P/LP) missense variants are located in the MH2 domain [24].

Heterozygous P/LP variants in *SMAD3* (OMIM 603109) cause Loeys-Dietz Syndrome type 3 (LDS3, OMIM 613795, ORPHA 284984), also known as aneurysms-osteoarthritis syndrome (AOS). LDS3 is characterized by aneurysms and tortuosity of the aorta and/or middle-sized arteries, accompanied by osteoarthritis [5, 6]. Currently, over 60 different P/LP variants in *SMAD3* have been identified in LDS3 families [24–28], including missense, truncating and splicing variants, and intragenic and whole gene deletions [24, 29, 30]. Interestingly, large phenotypic variation is described between LDS3 families, suggesting that, among others, genotype and ancestry might play a role. Hostetler *et al*. showed that an aortic event occurred at younger age in individuals with a DN variant in the MH2 domain of SMAD3 compared to individuals with a HI variant in the MH2 domain or a variant in the MH1 domain [31]. In addition, variability in severity of the phenotype is observed within families [5, 32], which indicates that the severity of LDS3 is influenced by other factors, including genetic modifiers [33], lifestyle, co-morbidities, and/or sex.

Besides P/LP *SMAD3* variants, variants of unknown significance (VUS) are often found in *SMAD3*. In our centre, 13 out of 50 unique *SMAD3* variants (26%) discovered upon diagnostic testing were classified as VUS, including 10 variants found in syndromic TAA patients and 3 variants in non-syndromic TAA patients (unpublished data). Improving the interpretation of the pathogenicity of these *SMAD3* VUS is essential, since the molecular genetic diagnosis is important for appropriate management and treatment of the patient and allows for predictive genetic testing in family members at risk. A molecular genetic diagnosis of LDS3 guides the frequency and extent of vascular imaging and the threshold for preventive surgery [34]. The vast amount of VUS found in genetic testing as well as the clinical utility of a certain diagnosis of LDS3, underlines the need for assays to functionally characterize and interpret *SMAD3* variants.

Here, we studied the effect of P/LP and VUS *SMAD3* variants by performing functional experiments on patient-derived in vitro differentiated fibroblasts (myofibroblasts) and VSMCs. Myofibroblasts differentiation can be a more accessible cell model to study patient-related variants compared to VSMCs, since VSMCs can only be obtained during surgery. In these functional cell-based experiments, we analyzed the differentiation potential, activation of the TGF-β pathway, the expression of SMC markers, and the formation of ECM.

Results

Phenotype-genotype correlations

In our center, we identified 67 individuals with LDS3 from 12 families (Table 1 and Supplementary Table 1). Over half of the individuals (41/67, 61.2%) were heterozygous for a missense variant in the MH2 domain of *SMAD3*. Only one missense variant in the MH1 domain was reported (Table 1, Supplementary Table 1). In total, 37/67 individuals (55.2%) suffered from an aortic event, with an overall median age of 40.5 years [IQR 31.0–50.8]. The overall median age of individuals without an aortic event was 43.5 years [IQR 21.0–60.8]. Individuals with a missense variant in the MH2 domain of SMAD3 were more likely to experience an aortic event compared to individuals with an HI variant (66.7% versus 44.0% respectively, $P = 0.054$). The median age at aortic event for individuals with a missense variant in MH2 was 35.0 years [IQR 29.0–47.0], which, although not significantly different, was 11 years lower than the median age at aortic event for individuals with an HI variant (46.0 years [IQR 40.0–54.0], $P = 0.07$).

Effect of *SMAD3* HI and DN variants on the protein level/structure

The *SMAD3* variants and cell lines studied are depicted in Supplementary Table 2. Variant p.Phe248Profs*62 (FB#3) and the deletion of a large part of *SMAD3* (VSMC#7) are expected to result in HI [6]. Based on the protein structure of the SMAD3/SMAD4 complex, we expected *SMAD3* variant p.Arg287Trp (VSMC#1-6 and FB#1-2) and p.Arg268Cys (FB#4) to have a DN effect since the change in the SMAD3 protein structure will affect the stability and formation of the SMAD3-SMAD3-SMAD4 protein complex. The interruption of the protein complex is due to a loss of positive charge, the bulky side chain of tryptophan, and potential loss of H-bridges at the interaction site (Fig. 1A). The variant p.Ile396Thr (FB#5) was classified as VUS and is expected to have a DN effect. This variant is not close to the interaction site and is expected to reduce the stability of the SMAD3 protein (Fig. 1A). DNA restriction analysis confirmed the expected mutant allele in all cell lines with a *SMAD3* missense variant (Fig. 1B and C). No mutant allele is present in the haploinsufficient cell line FB#3 p.Phe248Profs*62, since the expression of the mutant allele will be very low or absent due to nonsense-mediated decay (NMD) [6].

TGF-β induced differentiation and functional analysis of patient-derived fibroblasts

Initial activation of the TGF-β pathway in SMAD3 fibroblasts is not affected

TGF-β signaling activity was determined by performing western blots for SMAD2, pSMAD2, SMAD3 and pSMAD3 at different time points after TGF-β stimulation (Fig. 2). All cell lines showed induction of SMAD2 and SMAD3 phosphorylation after TGF-β stimulation. Phosphorylated SMAD2 and SMAD3 reached their highest levels 30–60 min after TGF-β stimulation. These data indicate that initial activation of the TGF-β pathway can still occur in cell lines with *SMAD3* variants. As expected, FB#3 p.Phe248Profs*62 showed reduced expression of SMAD3 (Fig. 2D). Although pSMAD3/SMAD3 ratios were unaltered in this HI cell line, the results do show that the absolute SMAD3 and pSMAD3 protein levels were lower. Due to NMD, this reduction is expected for HI variants and could lead to a lower downstream TGF-β signaling response.

Reduced differentiation potential of fibroblasts with DN SMAD3 P/LP variants

During patient fibroblast culture, the morphology of *SMAD3* patient fibroblasts appeared to differ from controls (Supplementary Fig. 1). The *SMAD3* patient fibroblasts have a rounded morphology, while control fibroblasts have a more continuous and stretched morphology. The differences in morphology

Table 1. Genotype-phenotype correlations.

	Missense MH1 domain (n = 1)	Missense MH2 domain (n = 41)	Haploinsufficient (n = 25)	MH2 vs HI P-value
Median age at aortic event (years)	-	35.0 [29.0–47.0]	46.0 [IQR 40.0–54.0]	0.065
Aortic event (% of total) (n = 37)	0	26 (66.7%)	11 (44.0%)	0.054
Median age no aortic event (years)	75	48.5 [28.25–63.75]	34.0 [19.5–54.5]	0.084
Sudden death (% of total) (n = 17)	0	8 (20.5%)	9 (36.0%)	0.171
Osteoarthritis (% of total) (n = 36)	0	28 (71.8%)	8 (32.0%)	0.005

between *SMAD3* patient cells and controls were still present after differentiation into myofibroblasts (Supplementary Fig. 1).

The differentiation potential of patient fibroblasts compared to controls was assessed by quantitative analysis of SMA positive cells after transdifferentiation (Fig. 3A). Western blotting showed a SMA expression below the 1xSD range of the controls in FB#1 p.Arg287Trp and FB#2 p.Arg287Trp. In contrast, the SMA expression in FB#3 p.Phe248Profs*62 was significantly increased compared to all other cell lines ($P = < 0.0001$–0.0097) (Fig. 3B and C). SMA expression in VUS FB#5 p.Ile396Thr was slightly above the 1× SD range, but do not significantly differ from controls ($P = 0.9968$) (Fig. 3B and C). Furthermore, the Western blots indicate that SM22 expression is reduced in FB#1 p.Arg287Trp, FB#2 p.Arg287Trp and FB#4 p.Arg268Cys, although this reduction is not significant (Fig. 3B and D). In contrast, expression of SM22 in FB#3 p.Phe248Profs*62 was significantly increased (Fig. 3B and D).

FB#1 p.Arg287Trp, FB#2 p.Arg287Trp and FB#4 p.Arg268Cys myofibroblasts visually showed a reduction of SMA expression in immunofluorescence (Fig. 3E). This reduction was confirmed by quantification (Fig. 3F), with a mean SMA expression below the 1x SD range ($P < 0.0001$–0.0003). The decrease in SMA expression of VUS FB#5 p.Ile396Thr was not significant ($P = 0.3066$). However, since the SMA expression of the VUS is below the 1x SD, the variant is not expected to be HI. On the other hand, FB#3 p.Phe248Profs*62 showed a significant increase in SMA expression compared to controls ($P < 0.0001$) as well as to the other *SMAD3* cell lines ($P < 0.0001$). Quantification of SM22 IF staining did not show significant differences (data not shown). Of note, fibroblasts that were not stimulated by TGF-β showed almost no SMA expression and low SM22 expression (data not shown).

In conclusion for this dataset, SMA and SM22 Western blots and immunofluorescence staining indicate a decreased differentiation potential in DN cell lines FB#1 p.Arg287Trp, FB#2 p.Arg287Trp and FB#4 p.Arg268Cys. In contrast, HI cell line FB#3 p.Phe248Profs*62 showed an increased differentiation potential. VUS cell line FB#5 p.Ile396Thr also showed a reduction of SMA expression assessed by IF staining, although less pronounced compared to the pathogenic DN SMAD3 variants.

In addition, the expression of contractile marker MYH11 and synthetic marker vimentin in myofibroblasts was analyzed (Supplemental Fig. 2), which did not show significant differences.

Differentiated DN SMAD3 myofibroblasts show decreased fibrillin-1 ECM deposition

We examined the fibrillin-1 ECM deposition of myofibroblasts from *SMAD3* patients and controls after 7 days of culture (Fig. 4).

All cells did show some expression of fibrillin-1, however the DN cell lines show less elongated fibers compared to the controls and HI cell lines.

Functional assays in vascular smooth muscle cells

An HI SMAD3 P/LP variant promotes the expression of contractile marker SMA

To examine whether VSMCs behave similarly as myofibroblasts, VSMCs of *SMAD3* patients and controls were characterized by staining for contractile and synthetic VSMC markers (Fig. 5). The expression of contractile marker SMA in HI *SMAD3* VSMC #7 clearly exceeded the 1× SD range of controls on Western blot and was significantly increased compared to controls and DN *SMAD3* VSMCs (Fig. 5A and B). This increased SMA expression was confirmed by IF (Fig. 5D and E). The SMA expression of the DN *SMAD3* VSMCs was within the 1x SD range and did not significantly differ from controls (Fig. 5D and E). Although SM22 expression of HI VSMC #7 exceeded the 1x SD range for controls on Western blot, this difference was not significant (Fig. 5A and C). In addition, quantification of the SM22 staining did not show significant differences (data not shown). Furthermore, Western blot did not show clear differences in vimentin expression, a marker for synthetic VSMCs (Supplemental Fig. 3).

A HI *SMAD3* P/LP variant promotes the expression of different *MYH11* isoforms in VSMCs

Another marker for contractile VSMCs is MYH11. Western blot showed increased MYH11 expression for HI *SMAD3* VSMC #7 compared to controls and DN *SMAD3* VSMCs (Fig. 6A), which was confirmed with IF (Fig. 6B). The expression of *MYH11* in DN *SMAD3* VSMCs (VSMC #1-6) was similar to controls. DNA sequencing of *MYH11* was performed to examine whether the increased MYH11 expression was caused by a *MYH11* P/LP variant. However, no alterations in *MYH11* were observed. Interestingly, the increased MYH11 expression in HI VSMC #7 seems to be caused by expression of a larger MYH11 protein isoform. Different isoforms of *MYH11*, caused by alternative splicing, are known to be expressed during embryonal development [35] and are indicated in Fig. 6C. A PCR analysis of cDNA prepared from control VSMC A and VSMC #7 indicated different expression levels of the *MYH11* isoforms in VSMC #7, with highest expression of isoform SM1A (Fig. 6D, Table 2). This was confirmed by splice analysis on RNA sequencing data in VSMC #7 and VSMC A, revealing alternative splicing of exon 5b (5′ end) and the exon generating the short carboxyl terminus (3′ end) in VSMC #7

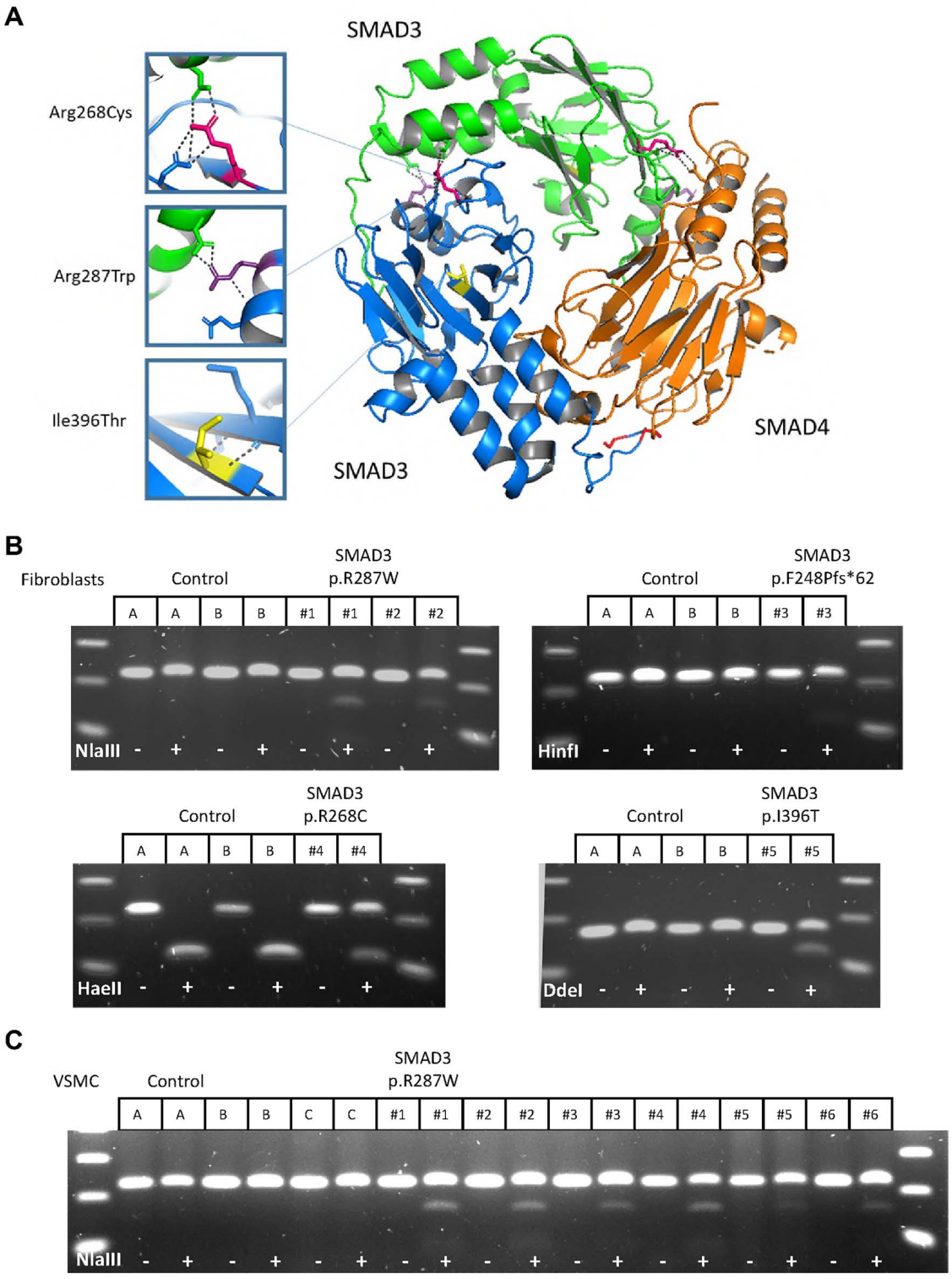

Figure 1. SMAD3 mutations. (A) Protein structure of two MH2 domains of SMAD3 (blue and green) which form a protein complex together with a MH2 domain of SMAD4 (orange). Locations of DN SMAD3 mutations in patient cell lines are indicated. p.Arg287Trp (purple) and p.Arg268Cys (pink) will change the charge of the amino acid and are located near the interaction side, which will likely affect interactions between proteins and stability of the protein complex. p.Ile396Thr (yellow) will probably affect stability of protein structure. Image of PDB file 1U7F [55] created with PyMol [56]. (B) Restriction analysis of PCR product on cDNA fibroblasts. (C) Restriction analysis of PCR product on cDNA VSMCs.

(Fig. 6E). Based on the number of alternative splicing events causing exclusion of both exons, isoform SM1A is expected to be most expressed (Fig. 6F). Expression of isoform SM1A results in a protein with a length of 1972 amino acids, which is the second largest isoform of MYH11. This can explain the additional band observed on Western blot indicating the expression of a larger MYH11 isoform compared to control VSMCs.

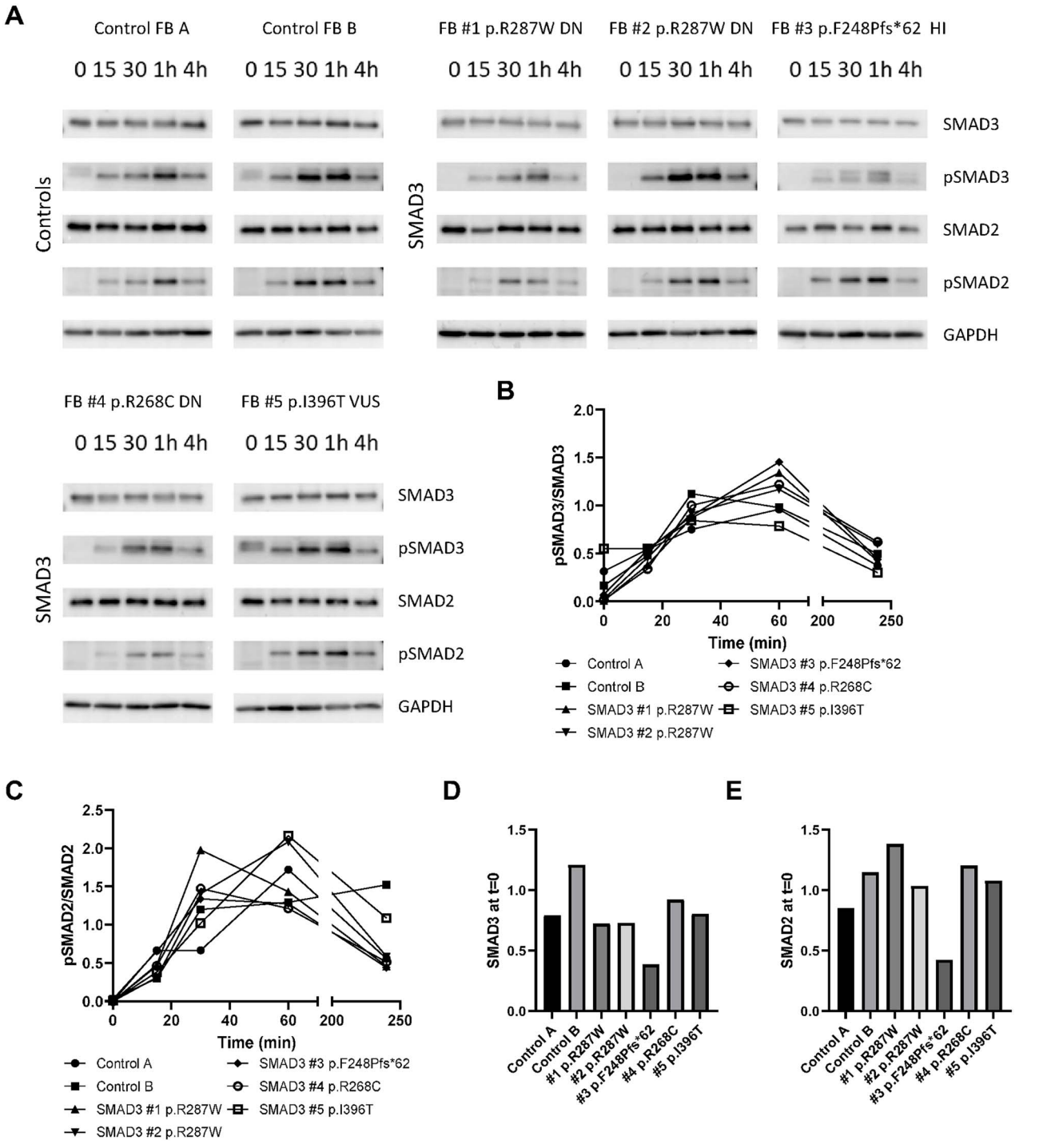

Figure 2. Downstream transcriptional activation of TGF-β signaling in SMAD3 fibroblasts. (A) Western blots detecting pSMAD3, SMAD3, pSMAD2, and SMAD2 in fibroblasts upon stimulation with TGF-β (15 min, 30 min, 1 h, and 4 h) after serum deprivation. GAPDH levels serve as a loading control. (B) Quantification of pSMAD3/SMAD3 ratio. (C) Quantification of pSMAD2/SMAD2 ratio. (D) SMAD3 levels at t = 0. (E) SMAD2 levels at t = 0.

SMAD3 mutated VSMCs show delayed fibrillin-1 deposition

We examined the deposition of ECM component fibrillin-1 of VSMCs from *SMAD3* patients and controls after 7 days (Fig. 7) and after 14 days (Supplemental Fig. 4).

Fibrillin-1 staining was mainly reduced in *SMAD3* VSMC #3, #5, #6 p.Arg287Trp after 7 days (Fig. 7) and VSMC #4 seems to form more fibrillin-1. After 14 days, all cell lines show comparable ECM deposition (Supplemental Fig. 4B).

Discussion

Functional assays on patient-derived differentiated fibroblasts and VSMCs with a P/LP variant in *SMAD3* were performed in order to elucidate the molecular and cellular effects of these *SMAD3* variants, to improve interpretation of VUS. There is an unmet need for a fast and reliable readout in the diagnostic setting, since the number of identified VUS is growing and adequate interpretation of these VUS is essential for patient management. Besides, the comparison of the assays of these two cell types will

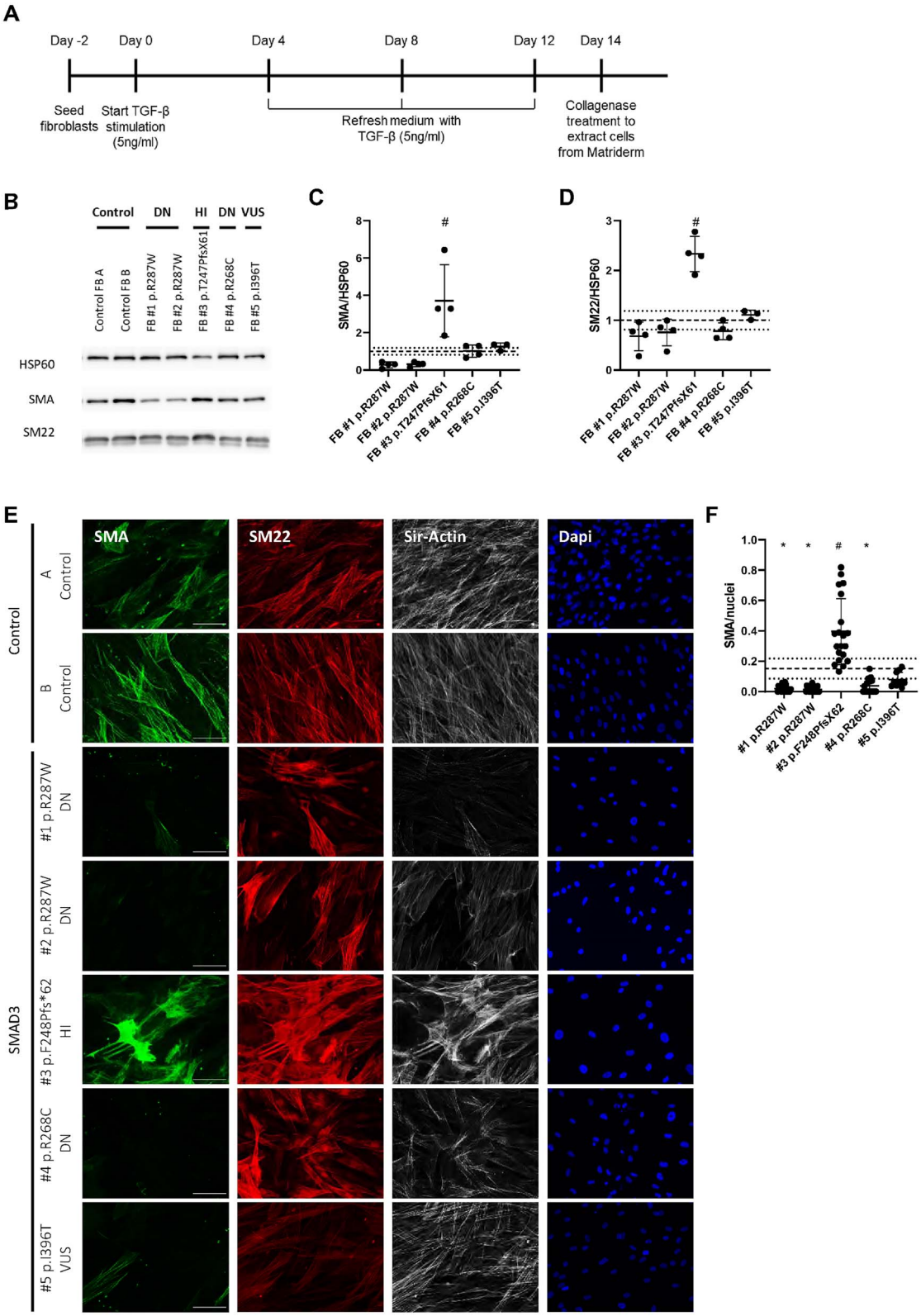

Figure 3. Transdifferentiation potential of SMAD3 fibroblasts is reduced. (A) Time line of TGF-β induced transdifferentiation of fibroblasts. (B) Western blots detecting SMA and SM22 in transdifferentiated fibroblasts. HSP60 levels serve as a loading control. (C) Quantification of SMA levels in B. (D) Quantification of SM22 levels in B. (E) Immunofluorescent staining of SMA (green), SM22 (red), F-actin (gray) and DAPI (blue) after 14 days of transdifferentiation of SMAD3 fibroblasts and controls. Scale bar represents 100 μm. (F) Quantification of SMA positive cells divided by the total number of nuclei. Grey dashed line represents the mean of the controls and black dotted lines represent 1x SD range of the controls. The 1xSD range represents the normal variation of controls. *significantly decreased compared to controls. #significantly increased compared to controls and other SMAD3 cell lines.

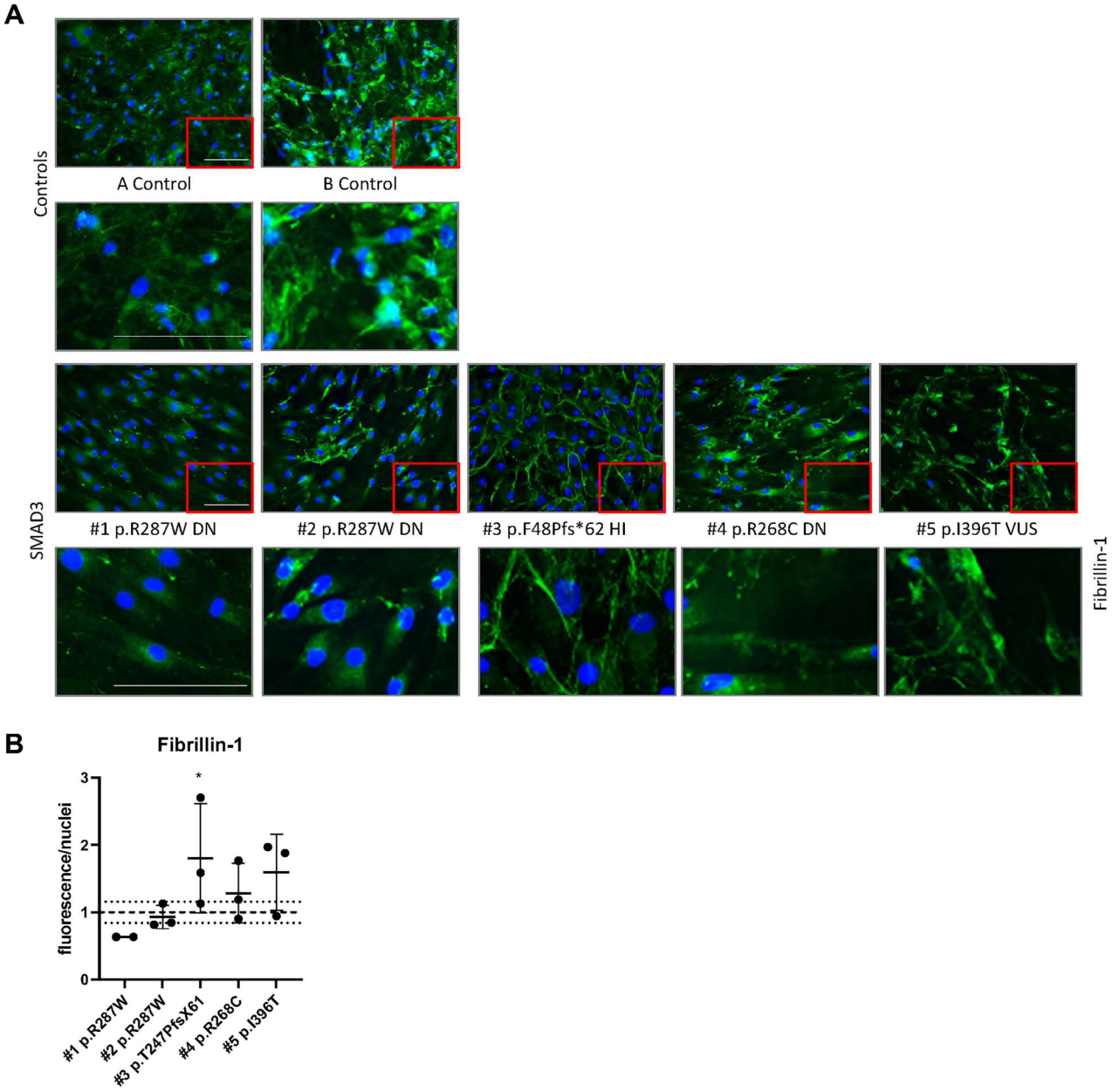

Figure 4. ECM proteins in transdifferentiated fibroblasts. (A) Fibrillin-1 staining after 7 days of culture. (B) Quantification of Fibrillin-1 staining. Scale bar represents 100 μm. *significantly increased compared to controls.

provide further insight into the reliability of using differentiation of fibroblasts instead of VSMCs, as patient fibroblasts are more easily accessible. A summary of the molecular and cellular characteristics established in this study is provided in Table 3.

The differentiation potential of myofibroblasts differed between different types of *SMAD3* variants. A strong reduction is seen in SMA expression after differentiation into myofibroblasts in the DN *SMAD3* myofibroblasts, which is in line with previous results obtained for FB#1 p.Arg287Trp [36]. In contrast to the DN *SMAD3* myofibroblasts, HI *SMAD3* myofibroblasts show an increased differentiation potential. Hence, not all *SMAD3* variants affect differentiation into myofibroblasts after TGF-β stimulation to the same extent, which might point to a different underlying molecular disease mechanism for DN and HI *SMAD3* variants.

The expression of contractile markers SMA and SM22 was increased in HI *SMAD3* VSMCs, while there is no significant difference in DN *SMAD3* VSMCs compared to controls. The synthetic marker vimentin is not reduced in those cells, indicating that despite an increase in contractile markers there is no clear shift towards the contractile phenotype.

The ECM formation is less structured in DN *SMAD3* myofibroblasts for fibrillin-1 compared to HI *SMAD3* myofibroblasts. This finding is interesting, since P/LP variants in genes involved in formation and integrity of the ECM, like Fibrillin-1, generally lead to ECM accumulation. Furthermore, ECM components are still formed in VSMCs, but the formation seems to be delayed in some DN *SMAD3* VSMCs. This is in line with previous findings for Smad3 mouse models [37–39]. The reduced ECM formation is likely caused by dysregulation of the downstream TGF-β pathway. This dysregulation reduces downstream transcription of genes, including ECM components and matrix metalloproteases (MMPs), which are important for matrix remodeling. The reduced

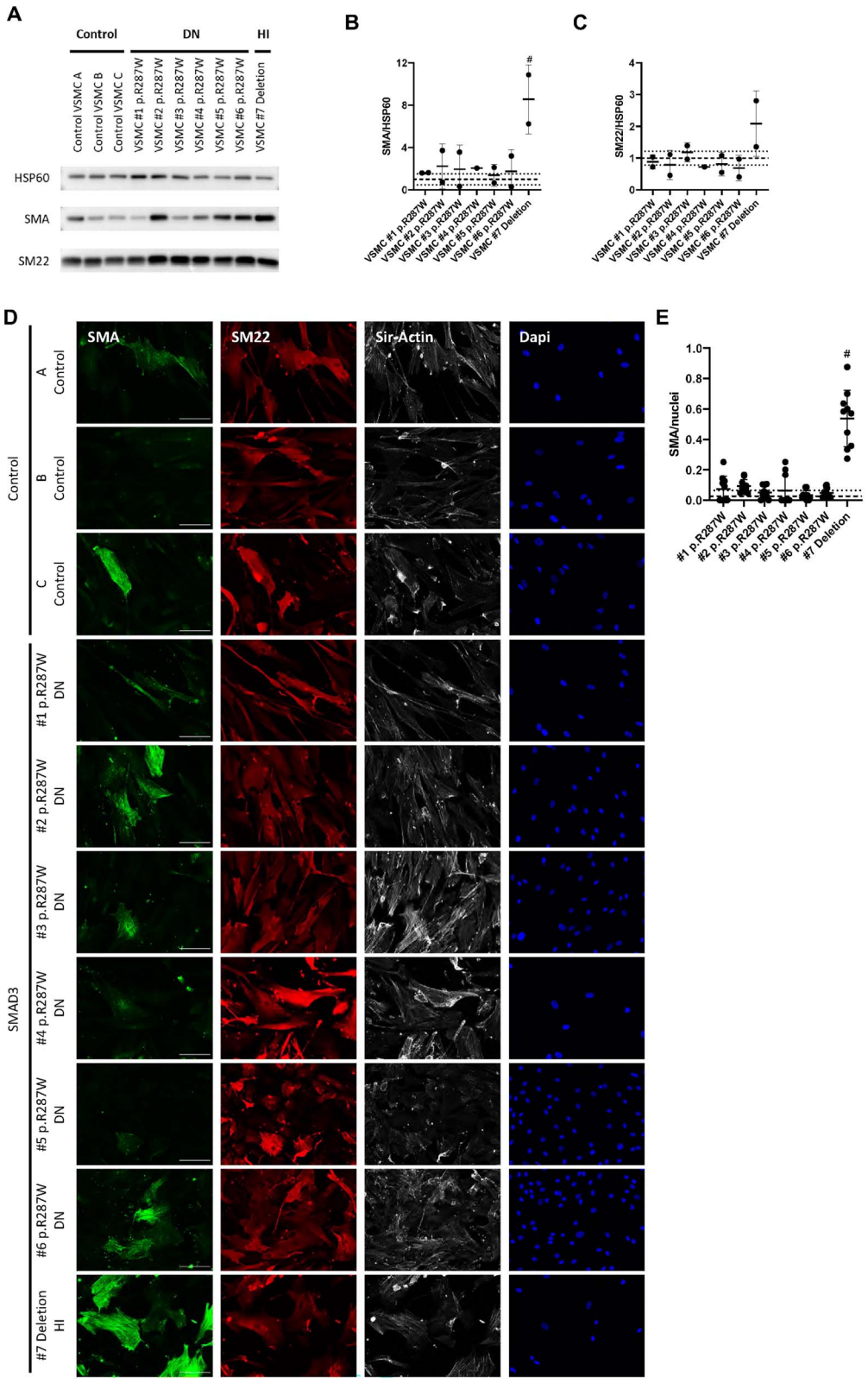

Figure 5. VSMC characterization. (A) Western blots detecting SMA and SM22 in VSMCs. HSP60 levels serve as a loading control. (B) Quantification of SMA levels in A. (C) Quantification of SM22 levels in A. (D) Immunofluorescent staining of SMA (green), SM22 (red), F-actin (gray) and DAPI (blue) of SMAD3 VSMCs and controls. Scale bar represents 100 μm. (E) Quantification of SMA positive cells divided by the total number of nuclei. Grey dashed line represents the mean of the controls and black dotted lines represent 1x SD range of the controls. # significantly increased compared to controls and other SMAD3 cell lines.

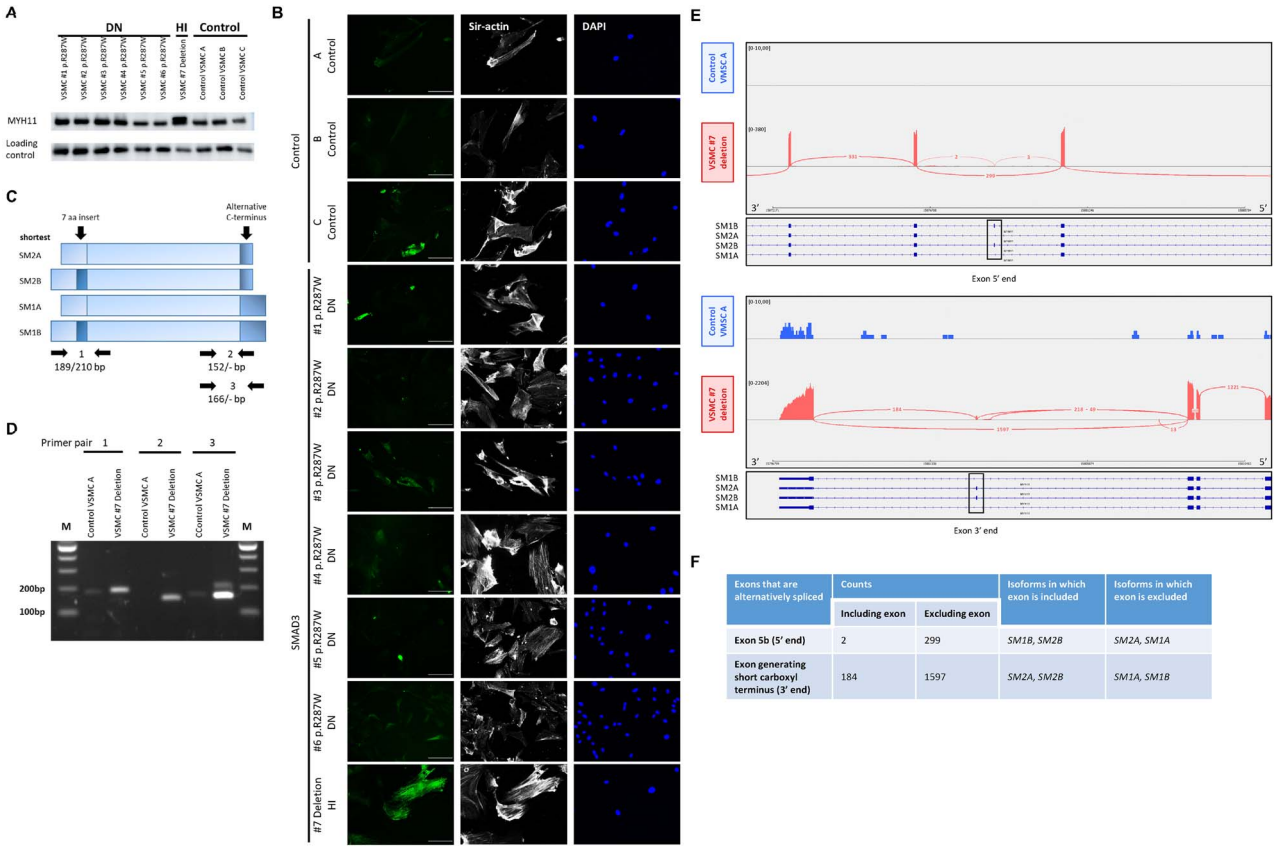

Exons that are alternatively spliced	Counts		Isoforms in which exon is included	Isoforms in which exon is excluded
	Including exon	Excluding exon		
Exon 5b (5′ end)	2	299	*SM1B, SM2B*	*SM2A, SM1A*
Exon generating short carboxyl terminus (3′ end)	184	1597	*SM2A, SM2B*	*SM1A, SM1B*

Figure 6. MYH11 expression in VSMCs. (A) Western blot detecting MYH11 in VSMCs. B-catenin levels serve as a loading control. (B) Immunofluorescent staining of MYH11 (green), F-actin (gray) and DAPI (blue) of SMAD3 VSMCs and controls. Scale bar represents 100 μm. (C) Schematic representation of different MYH11 isoforms caused by alternative splicing. Indicated the primer pairs to perform PCRs on cDNA to detect different isoforms. (D) PCR on cDNA to detect different isoforms of MYH11 in control VSMC A and SMAD3 VSMC #7 deletion. Table 3 gives an overview of expected sizes of PCR products for the different isoforms. (E) Sashimi plot for the alternatively spliced exons on the 5′ end and 3′ end of the MYH11 gene in patient VSMCs (#7 deletion) and control VSMCs. Per-base expression is plotted on the y-axis of the sashimi plot and genomic coordinates on the x-axis. The four different isoforms of MYH11 (SM1B, SM2A, SM2B and SM1A) are indicated below the sashimi plot. Alternative splicing events of both exons are detected in the patient VSMCs, whereas none are detected in the control VSMCs. (F) Table showing the number of splice events resulting in either inclusion or exclusion of the exon on the 5′ end and the exon on the 3′ end of MYH11. Since the largest number of splice events result in exclusion of both the exon on the 5′ end and the exon on the 3′ end, isoform SM1A is expected to be most expressed.

Table 2. Primer pairs and expected sizes MYH11 isoforms.

Primer pair	Primer forward	Primer reverse	Size (bp)
1	5′-GAGTCTGGAGCCGGGAAAAC-3′	5′-TCGTGAGGAGTTGTCGTTCTT-3′	SM2A: 189 SM2B: 210 SM1A: 189 SM2B: 210
2	5′-GGAGTCCCAGCGCATCAA-3′	5′-TGGTGCATCACTGCGAAGTTT-3′	SM2A: 152 SM2B: 152 SM1A: - SM2B: -
3	5′-GGAGTCCCAGCGCATCAA-3′	5′-GGAGTCCCAGCGCATCAA-3′	SM2A: - SM2B: - SM1A: 166 SM2B: 166

transcription of ECM components and MMPs disrupts sufficient ECM formation and weakens the aortic structure.

SMAD2 and SMAD3 phosphorylation was not altered in LDS3 patient-derived fibroblasts after TGF-β stimulation. This indicates that initial activation of the TGF-β pathway can still occur in cell lines with P/LP *SMAD3* variants with either DN or HI effect. The antibodies for SMAD3 and pSMAD3 recognize the part of SMAD3 where the P/LP variants are not located and the P/LP variants are not expected to alter the phosphorylation sites. Therefore, the absence in different phosphorylation between healthy and mutated SMAD3 will not be caused by the action of the antibodies.

Comparison of functional assays between myofibroblasts and VSMCs

We compared the differentiation potential and ECM formation between fibroblasts differentiated into myofibroblasts and

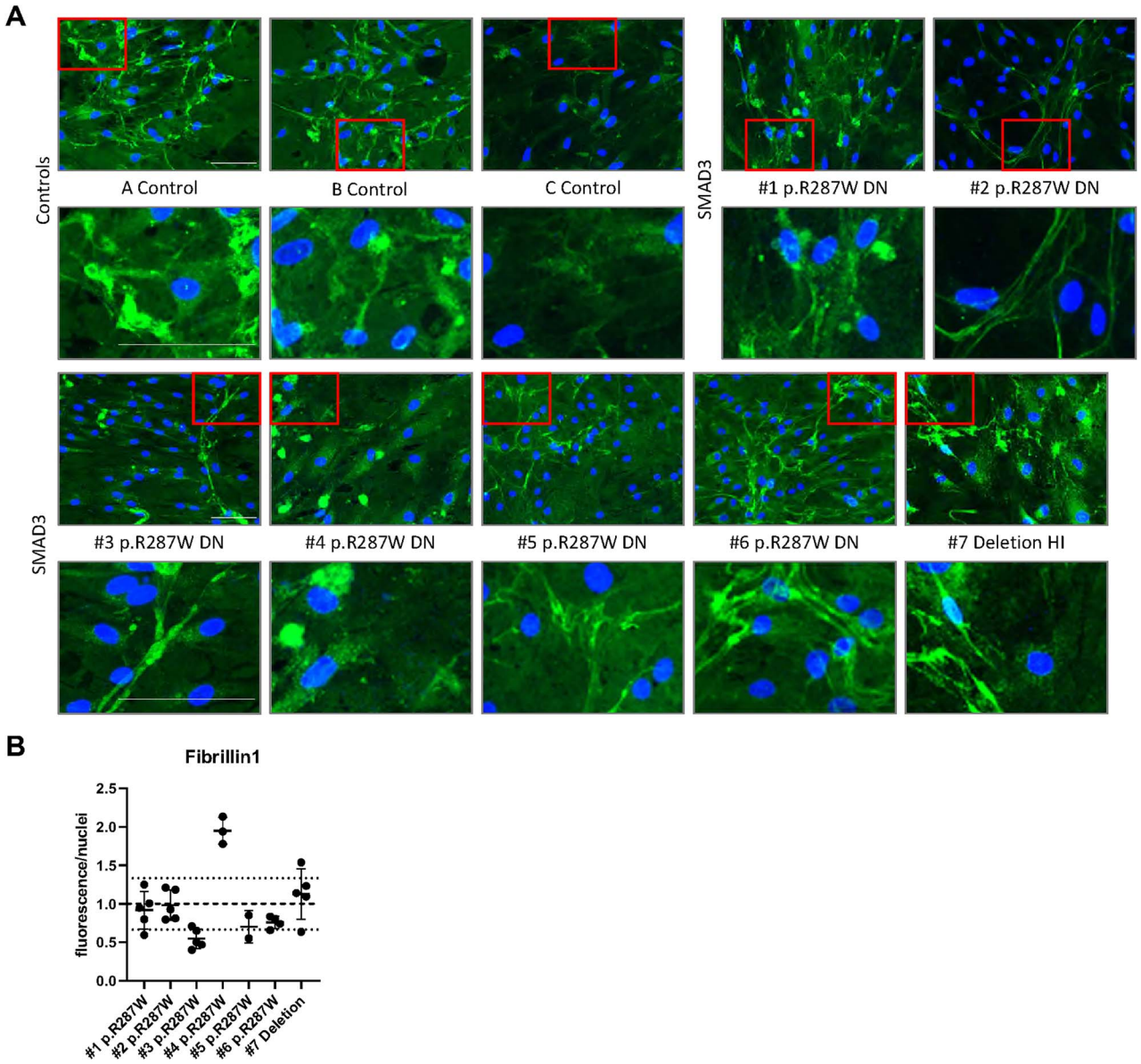

Figure 7. ECM proteins in VMSC. Immunofluorescent images show deposition of ECM components after 7 days of culture. Scale bar represents 100 μm. (A) Fibrillin-1 staining. (B) Quantification of Fibrillin-1 staining.

VSMCs, to examine whether myofibroblasts are an alternative model to study the molecular mechanism of *SMAD3* variants.

The SMA and SM22 expression patterns were equal for HI *SMAD3* myofibroblasts and VSMCs. In contrast, SMA and SM22 expression was reduced in DN *SMAD3* myofibroblasts compared to controls and not in VSMCs. Besides, myofibroblasts showed a reduced elongated fibrillin-1 fiber formation in DN *SMAD3* cell lines compared to controls, whereas no differences in ECM formation were observed in either DN *SMAD3* VSMCs or HI *SMAD3* VSMCs compared to controls.

The different origin of fibroblasts and VSMCs might explain the different outcomes in SMA and SM22 expression and ECM formation between these cell types. VSMCs are isolated from different parts of the aorta, while fibroblasts are all obtained from the inner side of the upper arm. Dermal fibroblast in the upper arm all have the same embryonic origin, namely the lateral plate mesoderm [40]. Additionally, it is important to realize that the embryonic origin can vary between VSMCs, since the aorta is derived from distinct embryonic sources. The ascending aorta is derived from neural crest (NC), whereas the descending aorta originates from somatic mesoderm [41]. Several studies suggest that individual VSMC characteristics, including gene expression, are determined by the embryonic origin [42–44]. Besides the embryonic origin, the region of the aorta can contribute to the VSMC characteristics, since previous studies have shown that the VSMC characteristics differ based on the location in the vascular tree [44]. Furthermore, VSMCs play an important role in arterial remodelling to maintain arterial structure and function [45]. Due to biomechanical and biochemical stressors, VSMCs will lose contractile markers and differentiate to a synthetic VSMC phenotype to induce proliferation and migration [46]. The different embryonic origins of VSMCs and phenotypic switch under biological stress signals might influence the results not only between fibroblasts and VSMCs but also between different VSMCs lines. Therefore, large numbers of VSMCs are needed to examine whether specific results are based on phenotypic

switches or due to a genetic variant. In conclusion, functional assays for differentiation potential and ECM formation can distinguish between DN and HI *SMAD3* variants. Differentiation of fibroblasts seems to be a more suitable method for these functional assays as an alternative for VSMCs. Besides, potential interventions may need to be tailored based on the specific cell type and microenvironment involved, given that the observed differences between fibroblasts and VSMCs can be due to embryonic origin, regional influences, or stress responses. This knowledge could therefore guide the development of more effective and precise therapeutic strategies for addressing vascular complications in the different patient populations.

Differences between HI and DN *SMAD3* variants

The expression of VSMC markers showed opposing results for DN and HI *SMAD3* mutant cells; SMA and SM22 expression is reduced in DN *SMAD3* variants and increased in HI *SMAD3* variants. This suggests that there might be a different effect on the TGF-β and bone morphogenetic protein (BMP) signalling within the cells. BMP signaling plays an important role in vascular remodeling, maintenance of joint integrity, the initiation of fracture repair, among others [47]. The TGF-β pathway signaling can occur via a canonical or non-canonical route. The canonical route includes two pathways, namely via TGF-β ligands and via BMP ligands. If the TGF-β canonical pathway is activated by TGF-β ligands, SMAD4 forms complexes with SMAD2/3. If activated by BMP ligands, SMAD4 forms complexes with SMAD1/5/8 (R-SMADs). We speculate about the role of SMAD4 in the different effects of DN and HI variants, since SMAD4 is present in the canonical TGF-β signaling and the BMP signaling pathway. The phosphorylation of SMAD1/5/8 is indirectly induced by BMPs. Phosphorylated SMAD1/5/8 associates with SMAD4 and regulates gene expression in the cell nucleus. If more SMAD4 is available, more complexes with SMAD1/5/8 will be formed resulting in more gene regulation via the BMP signaling. Since only half of the SMAD3 protein is available in cells with HI SMAD3 variants, a reduced amount of complexes with SMAD4 will be formed. This will result in less "trapped" SMAD4 and thus a larger amount of freely available SMAD4 to form complexes with SMAD1/5/8 and regulate downstream genes, including *SMA*. The increased regulation of downstream genes might explain the increased differentiation potential in HI *SMAD3* mutated cells compared to controls and DN *SMAD3* mutated cells.

MYH11 isoforms

A strongly increased *MYH11* expression was only noticed in the HI *SMAD3* VSMC and seems to be caused by the expression of an additional protein isoform. Four different isoforms are known for MYH11; the expression of which differs during embryonic development and varies between tissue types [35]. The SM1 isoforms are mostly present in the embryonic stage, whereas the SM2/SM1 ratio increases during cell maturation. PCRs and RNA sequencing confirmed the altered expression of *MYH11* isoforms in the HI *SMAD3* VSMC. The SM1A isoform that is normally present during embryonic development is probably most abundant. We hypothesize that the altered expression of MYH11 isoforms might be a result of altered *SMAD3* expression, since these HI VMSCs did potentially undergo a different maturation/differentiation process compared to controls and to *SMAD3* cell lines with a DN P/LP variant. Another hypothesis is based on the knowledge that tissues can revert to embryonic characteristics during stress. Reverting to the embryonic developmental program gives cells of a specific organ the ability to repair and maintain function, which is previously shown in for example heart tissue [48, 49]. Due to the presence of a HI *SMAD3* P/LP variant, these VSMCs have endured stress and might be reverted to their embryonic developmental program. The HI myofibroblast cell line did not show altered expression of *MYH11*, which is possibly caused by the very low *MYH11* expression in fibroblasts [50]. As we only had VMSCs of one HI *SMAD3* patient, we were not able to reproduce these data in independent HI *SMAD3* VSMC lines.

Correlation between phenotypic variability and VSMC markers

Phenotype-genotype correlations between HI and DN P/LP *SMAD3* variants are previously studied by Hostetler *et al.* in 212 individuals with a P/LP *SMAD3* variant [31]. Individuals with a DN *SMAD3* variant in the MH2 domain were significantly younger at first aortic event compared to those with a DN variant in the MH1 domain or a HI variant. Our retrospective analysis in *SMAD3* individuals seems to confirm the observations of Hostetler *et al.* [31]. The phenotypic variability between DN and HI variants might in part be explained by the different underlying molecular mechanisms like the observed opposite expression of VSMC markers between DN and HI myofibroblasts.

Unfortunately, we were not able to determine the pathogenicity of the VUS based on the differentiation potential and ECM formation. The characteristics of the VUS fibroblasts were intermediate between those of the controls and P/LP DN *SMAD3* variants and it is not possible to draw conclusions based on these small differences with the limited amount of available cell lines in this study. Therefore, an extension of this research including a larger number of cell lines is necessary to further investigate the SMA and SM22 expression and ECM formation in P/LP SMAD3 mutant cell lines. Moreover, it would be interesting to investigate whether the observed differences in SMA and SM22 expression and ECM formation is specific for P/LP *SMAD3* variants or whether these features are observed in other aneurysm genes as well.

Material and methods

Patient cells and characteristics

Primary dermal fibroblasts and VSMCs were collected from individuals with a P/LP variant or VUS in the *SMAD3* gene (NM_005902.4). In total, five *SMAD3* patient fibroblast cell lines, two control fibroblast cell lines (Biobank Clinical Genetics, Erasmus MC), seven *SMAD3* patient VSMC lines and three commercially available control VSMC lines were used (Lonza CC-2571, lot no. 0000369150, ATTC PCS-100-012, lot no. 62726859 and lot no. 64193202) (Supplementary Table 2). Collection of patient material was approved by the medical ethics committee of the Erasmus Medical Center Rotterdam (MEC 2014-579 and MEC 2017-040) and written informed consent was provided by all patients. A retrospective analysis was performed to obtain clinical data from the 12 individuals of the included samples (Supplementary Table 3). In addition, we reviewed the clinical and genetic data of all LDS3 67 individuals clinically examined in Rotterdam with a confirmed P/LP *SMAD3* variant, using the same methodology (Table 1, Supplementary Table 1). An aortic event was defined as an aortic dissection or surgical repair of an aortic aneurysm.

Cell culture

VSMCs were cultured in SmGM-2 medium supplemented with SMBM growth factors (Lonza, CC-4149 and CC-3181) in gelatin-coated dishes and incubated at 37°C with 5% CO_2. Fibroblasts were cultured in Dulbecco's Modified Eagle's Medium (DMEM,

Table 3. Overview characteristics transdifferentiated fibroblasts and VSMCs compared to controls.

	Expression VSMC markers								ECM formation			
	Western blot				Immunofluorescence				ECM staining			
	SMA	SM22	MYH11	Vimentin	SMA	SM22	MYH11	Vimentin	FibronectinFibrillin-1		Fibulin-4	Fibulin-5
TD fibroblasts												
DN	↓*	↓	~	~	↓*	↓	~	~	↓	↓	↓	↓
HI	↑*	↑*	~	~	↑*	↑	~	~	↑	~	~↑	~
VSMCs												
DN	~	~	~	~	~	~	~	~	~	~	~	~
HI	↑*	↑	↑*	~	↑	↑	↑	~	~	~	~	~

Summary of functional assays in transdifferentiated fibroblasts and VSMCs of individuals with a P/LP SMAD3 variant. TD; transdifferentiated, VSMCs; vascular smooth muscle cells, SMA; smooth muscle actin, SM22; smooth muscle 22, ECM; extra cellular matrix. Significant differences are visualized with *. No differences compared to controls is visualized with ~.

Table 4. Primers and expected sizes restriction analysis *SMAD3*.

SMAD3 variant	Restriction site change	Primer forward	Primer reverse	Fragment(s) WT allele (bp)	Fragment(s) mutated allele (bp)
p.Arg287Trp	Gain NlaIII site	5′-TTCACCGACCC CTCCAATTC-3′	5′-CAGCCATAGCG CTGGTTACA-3′	200	83, 117
p.Phe248Profs*62	Gain HinfI site	5′-CCGATGTCCCC AGCACATAAT-3′	5′-ACTGCTGCATTC CTGTTGACATT-3′	216	108, 108
p.Arg268Cys	Loss HaeII site	5′-TTCTGGTGCTCC ATCTCCTACTA-3′	5′-GAAGACCTCCCC TCCGATGTA-3′	106, 114	220
p.Ile396Thr	Gain DdeI site	5′-AGGGCTTTGAG GCTGTCTAC-3′	5′-CATCTGGGTGAG GACCTTGTC-3′	170	55, 115

Gibco, #11965-092) supplemented with 10% fetal calf serum (FCS, Capricorn, FBS-12A) and 1% penicillin/streptomycin (P/S, Sigma, P0781). The cultured fibroblasts were incubated at 37°C with 5% CO_2.

RNA isolation and cDNA

RNA was isolated from VSMCs with the RNeasy mini kit (Qiagen, #74104). cDNA was prepared with the iScript cDNA synthesis kit (Biorad, #170-8882) according to the manufacturer's protocol.

Restriction analysis

Restriction enzyme cleavage of PCR products derived from cDNA was performed to confirm the P/LP variants in these cell lines (Table 4). PCR on cDNA was performed with Q5 polymerase according to the manufacturer's protocol (Biolabs, M0493S). The PCR product was digested with an enzyme that gains or loses a restriction site due to the specific P/LP variant in that fragment (Table 4, NEB). Digestion was performed according to the manufacturer's protocol. After restriction, the products were separated on 2% agarose gels.

TGF-β stimulation

Cells were seeded in 6-well plates with DMEM, 1% P/S and 10% FCS to reach confluence. After 24 h, the medium was replaced by FCS-free medium. Cells were then stimulated with TGF-β for 0 min, 15 min, 30 min, 1 h and 4 h before collecting protein lysates. Lysis and western blotting were performed as described in the Western blotting protocol below.

Differentiation into myofibroblasts

Patient and control fibroblasts were differentiated into myofibroblasts as published [51] (Fig. 3A). In short, 250.000 fibroblasts were seeded in a 1 cm^2 piece of Matriderm (MedSkin Solutions, 83403-200). After 2 days, cells were attached and medium was replaced by DMEM with 2% heat-inactivated FCS, 1% P/S and 5 ng/ml active human recombinant TGF-β1 (Biovision, 4342-5). This medium was replaced every 4 days. At day 14, cells were enzymatically extracted from Matriderm by adding collagenase (2000 IU/ml, Worthington, LS004176) in DMEM with 10% FCS and 1% P/S and shaking at 37°C for 3 h. A centrifugation step was performed to remove collagenase before the myofibroblasts were seeded in new flasks and cultured in DMEM with 10% FCS and 1% P/S. After completion of the differentiation protocol, cells were used after 2–3 passages for functional assays. Passage number was kept below 5 to prevent loss of differentiation markers.

Western blotting

VSMCs and myofibroblasts were scraped in phosphate-buffered saline (PBS) supplemented with protease inhibitor cocktail (1:100, Roche, 11836145001) and phosphatase inhibitor cocktail (1:100, Sigma, P0044). These samples were lysed in equal volumes of 2× Laemmli buffer (4% SDS, 20% glycerol, 120 mM Tris pH 6,8) supplemented with protease inhibitor cocktail and phosphatase inhibitor. Lysates were passed through a 25G needle and heated to 65°C for 10 min. Protein concentrations were measured with Lowry protein assay [52]. Equal amounts of protein were separated on a SDS-PAGE gel and transferred to an Immobilon-P polyvinylidene difluoride (PDVF) membrane (Millipore, IPVH00010). Membranes were blocked in PBS with 3% milk powder (Sigma, 70166) and 0.1% Tween-20 (Sigma, P1379). After blocking, the membranes were incubated overnight in blocking buffer with primary antibody (Supplementary Table 4). Membranes were washed with 0,1% Tween-20 in PBS (5 times) and incubated for 1 h at room temperature (RT) with horseradish peroxidase-conjugated

secondary antibodies (1:2000, Jackson ImmunoResearch, 515-035-003 and 711-035-152). Membranes were washed again before protein detection, using home-made enhanced chemiluminescence (ECL) substrate on Amersham Imager 600 (GE Healthcare Life Sciences). Quantification of protein signals was performed using Fiji software [53].

Immunofluorescent staining

Subconfluent VSMCs (50%–70%) were grown on 18 mm coverslips in 12-well plates and fixed with 4% paraformaldehyde in PBS for 30 min. For immunostaining of differentiated fibroblasts, 100 000 skin fibroblasts/well were seeded on 18 mm coverslips in 12-well plates in DMEM with 10% FCS and 1% PS. After 2 days, medium was replaced by DMEM supplemented with 2% heat-inactivated FCS, 1% PS and 5 ng/ml human recombinant TGF-β1 (Biovision, 4342-5). This medium was changed every 4 days and after 14 days, cells were fixed with 2% paraformaldehyde in PBS for 15 min. After fixation, cells were permeabilized with PBS supplemented with 0.1% Triton-X-100 and blocked with PBS+ (PBS with 0.5% bovine serum albumin (BSA) and 0.15% glycine) for 30 min. Coverslips were incubated overnight at 4°C in PBS+ with primary antibodies: mouse monoclonal anti-smooth muscle actin (SMA) (1:750, Abcam, ab7817) and rabbit polyclonal anti-SM22 (1:400, Abcam, ab14106) or rabbit polyclonal anti-MYH11 (1:500, Abcam, ab53219) or rabbit monoclonal anti-vimentin (1:1000, Abcam, ab92547). Coverslips were washed with PBS supplemented with 0.1% Triton-X-100 and shortly with PBS+ before incubation with the secondary antibodies; anti-mouse Alexa Fluor 488 (1:1000, Molecular Probes, A11001) and anti-rabbit Alexa Fluor 594 (1:1000, Molecular Probes, A11012) and SiR-actin probe (1:1000, Cytoskeleton, SC001) in PBS+ for 1 h at room temperature. Coverslips were mounted in Vectashield with Dapi (Vector laboratories, H-1200,) and sealed with nail polish. Images were recorded with an Axio Imager D2 microscope (Zeiss).

Immunofluorescence of extracellular matrix

Cells were seeded at 50 000 cells/cm^2 in 8-well removable chamber slides (Ibidi, 80841) and grown for 7 days to allow ECM deposition. Cells were fixed with ice-cold 70:30 methanol: acetone mixture for 5 min and washed with PBS. Blocking was performed for 1 h in PBS supplemented with 10% normal goat serum (NGS) (Agilent, X0907). The cells were incubated overnight at 4°C with primary antibodies (Supplementary Table 5) in PBS + 10% NGS. After washing with PBS + 0.05%Triton X-100 (3 times for 5 min), the coverslips were incubated with a secondary antibody in PBS + 10% NGS for 1.5 h at ambient temperature (Molecular Probes, anti-rabbit Alexa Fluor 594, 1:1000, A11012). Coverslips were washed with PBS + 0.05% Triton X-100 and mounted to glass slides with Vectashield with DAPI (Vector laboratories, H-1200) and sealed with nail polish. Images were recorded with an Axio Imager D2 microscope (Zeiss).

PCR *MYH11* isoforms

Primers were designed for the different *MYH11* isoforms (Table 2). PCR on cDNA was performed with Q5 polymerase (NEB, M0491) according to the manufacturer's protocol. PCR products were separated on 2% agarose gels.

RNA sequencing and splice analysis

RNA was isolated from VSMCs as described above. Library preparation, sequencing and primary data analysis were performed at GenomeScan B.V. (Genomescan B.V., Leiden, The Netherlands). Libraries were paired-end sequenced in an Illumina Novaseq6000 platform at a sequencing depth of 40 million reads and 150 bp read length. Reads were aligned with the reference genome GRCh37.p13. To investigate alternative splicing of *MYH11*, sashimi plots were created in Integrative Genomics Viewer (IGV) [54]. Minimal junction coverage was set to two.

Statistics

Data were corrected for outliers with the Grubbs' test for outliers. Statistical analysis was performed with a non-parametric Mann–Whitney test. For a significant difference between groups the p-value must be < 0.05. In addition, the 1× standard deviation (SD) value of the controls is shown in the figures. All analyses were performed using Graphpad Prism, version 8.

Acknowledgements

We would like to thank Bianca de Graaf and Joyce Burger for isolating VSMC cell lines and Joyce Lebbink for analyzing the effects of variants on protein structure and the department of Clinical Genetics, laboratory diagnostics, for the preparation and storage of patient fibroblasts.

Supplementary data

Supplementary data is available at *HMG Journal* online.

Conflict of interest statement: None.

Funding

Nathalie P. De Wagenaar is funded by the Erasmus MC Mrace grant "SMAD3-Related Aneurysms-Osteoarthritis Syndrome; An integrative functional analysis of SMAD3 patient mutations to provide insight into genotype-phenotype relation, and recommendations for a clinical work-up".

References

1. Johnston KW, Rutherford RB, Tilson MD. *et al.* Suggested standards for reporting on arterial aneurysms. Subcommittee on reporting standards for arterial aneurysms, Ad Hoc committee on reporting standards, Society for Vascular Surgery and North American Chapter, International Society for Cardiovascular Surgery. *J Vasc Surg* 1991;**13**:452–8.
2. Melvinsdottir IH, Lund SH, Agnarsson BA. *et al.* The incidence and mortality of acute thoracic aortic dissection: results from a whole nation study. *Eur J Cardiothorac Surg* 2016;**50**:1111–7.
3. Verstraeten A, Luyckx I, Loeys B. Aetiology and management of hereditary aortopathy. *Nat Rev Cardiol* 2017;**14**:197–208.
4. Loeys BL, Chen JJ, Neptune ER. *et al.* A syndrome of altered cardiovascular, craniofacial, neurocognitive and skeletal development caused by mutations in TGFBR1 or TGFBR2. *Nat Genet* 2005;**37**:275–81.
5. van de Laar IM, van der Linde D, Oei EH. *et al.* Phenotypic spectrum of the SMAD3-related aneurysms-osteoarthritis syndrome. *J Med Genet* 2012;**49**:47–57.
6. van de Laar IM, Oldenburg RA, Pals G. *et al.* Mutations in SMAD3 cause a syndromic form of aortic aneurysms and dissections with early-onset osteoarthritis. *Nat Genet* 2011;**43**:121–6.
7. Boileau C, Guo DC, Hanna N. *et al.* TGFB2 mutations cause familial thoracic aortic aneurysms and dissections associated with mild systemic features of Marfan syndrome. *Nat Genet* 2012;**44**:916–21.

8. Bertoli-Avella AM, Gillis E, Morisaki H. *et al.* Mutations in a TGF-β ligand, TGFB3, cause syndromic aortic aneurysms and dissections. *J Am Coll Cardiol* 2015;**65**:1324–36.
9. Vorselaars VMM, Diederik A, Prabhudesai V. *et al.* SMAD4 gene mutation increases the risk of aortic dilation in patients with hereditary haemorrhagic telangiectasia. *Int J Cardiol* 2017;**245**: 114–8.
10. Micha D, Guo DC, Hilhorst-Hofstee Y. *et al.* SMAD2 mutations are associated with arterial aneurysms and dissections. *Hum Mutat* 2015;**36**:1145–9.
11. Cannaerts E, Kempers M, Maugeri A. *et al.* Novel pathogenic SMAD2 variants in five families with arterial aneurysm and dissection: further delineation of the phenotype. *J Med Genet* 2019;**56**:220–7.
12. Gillis E, Kumar AA, Luyckx I. *et al.* Candidate gene resequencing in a large bicuspid aortic valve-associated thoracic aortic aneurysm cohort: SMAD6 as an important contributor. *Front Physiol* 2017;**8**:400.
13. Doyle AJ, Doyle JJ, Bessling SL. *et al.* Mutations in the TGF-β repressor SKI cause Shprintzen-Goldberg syndrome with aortic aneurysm. *Nat Genet* 2012;**44**:1249–54.
14. Schepers D, Doyle AJ, Oswald G. *et al.* The SMAD-binding domain of SKI: a hotspot for de novo mutations causing Shprintzen-Goldberg syndrome. *Eur J Hum Genet* 2015;**23**:224–8.
15. Vander Ark A, Cao J, Li X. TGF-β receptors: in and beyond TGF-β signaling. *Cell Signal* 2018;**52**:112–20.
16. Hata A, Chen YG. TGF-β Signaling from receptors to Smads. *Cold Spring Harb Perspect Biol* 2016;**8**:a022061.
17. Miyazono K, ten Dijke P, Heldin CH. TGF-beta signaling by Smad proteins. *Adv Immunol* 2000;**75**:115–57.
18. Miyazono K. TGF-beta signaling by Smad proteins. *Cytokine Growth Factor Rev* 2000;**11**:15–22.
19. Heldin CH, Moustakas A. Role of Smads in TGFβ signaling. *Cell Tissue Res* 2012;**347**:21–36.
20. Massagué J. TGF-beta signal transduction. *Annu Rev Biochem* 1998;**67**:753–91.
21. Massagué J. TGFβ signalling in context. *Mol Cell Biol* 2012;**13**: 616–30.
22. Lindsay ME, Dietz HC. Lessons on the pathogenesis of aneurysm from heritable conditions. *Nature* 2011;**473**:308–16.
23. Macias MJ, Martin-Malpartida P, Massague J. Structural determinants of Smad function in TGF-beta signaling. *Trends Biochem Sci* 2015;**40**:296–308.
24. Schepers D, Tortora G, Morisaki H. *et al.* A mutation update on the LDS-associated genes TGFB2/3 and SMAD2/3. *Hum Mutat* 2018;**39**:621–34.
25. Keravnou A, Bashiardes E, Barberis V. *et al.* Identification of novel splice mutation in SMAD3 in two Cypriot families with nonsyndromic thoracic aortic aneurysm. Two case reports. *Mol Genet Genomic Med* 2020;**8**:e1378.
26. Richter JE Jr, Samreen A, Vadlamudi C. *et al.* Genomic observations of a rare/pathogenic SMAD3 variant in Loeys-Dietz syndrome 3 confirmed by protein informatics and structural investigations. *Medicina (Kaunas)* 2019;**55**:137.
27. Camerota L, Ritelli M, Wischmeijer A. *et al.* Genotypic categorization of Loeys-Dietz syndrome based on 24 novel families and literature data. *Genes (Basel)* 2019;**10**:764.
28. Engström K, Vánky F, Rehnberg M. *et al.* Novel SMAD3 p.Arg386Thr genetic variant co-segregating with thoracic aortic aneurysm and dissection. *Mol Genet Genomic Med* 2020;**8**: e1089.
29. Overwater E, Marsili L, Baars MJH. *et al.* Results of next-generation sequencing gene panel diagnostics including copy-number variation analysis in 810 patients suspected of heritable thoracic aortic disorders. *Hum Mutat* 2018;**39**:1173–92.
30. Hilhorst-Hofstee Y, Scholte AJ, Rijlaarsdam ME. *et al.* An unanticipated copy number variant of chromosome 15 disrupting SMAD3 reveals a three-generation family at serious risk for aortic dissection. *Clin Genet* 2013;**83**:337–44.
31. Hostetler EM, Regalado ES, Guo DC. *et al.* SMAD3 pathogenic variants: risk for thoracic aortic disease and associated complications from the Montalcino aortic consortium. *J Med Genet* 2019;**56**:252–60.
32. Chesneau B, Edouard T, Dulac Y. *et al.* Clinical and genetic data of 22 new patients with SMAD3 pathogenic variants and review of the literature. *Mol Genet Genomic Med* 2020;**8**:e1132.
33. Rahit K, Tarailo-Graovac M. Genetic modifiers and rare Mendelian disease. *Genes (Basel)* 2020;**11**:239.
34. Isselbacher EM, Preventza O, Hamilton Black J 3rd. *et al.* 2022 ACC/AHA guideline for the diagnosis and Management of Aortic Disease: a report of the American Heart Association/American College of Cardiology Joint Committee on clinical practice guidelines. *Circulation* 2022;**146**:e334–482.
35. Babu GJ, Warshaw DM, Periasamy M. Smooth muscle myosin heavy chain isoforms and their role in muscle physiology. *Microsc Res Tech* 2000;**50**:532–40.
36. Burger J, Bogunovic N, de Wagenaar NP. *et al.* Molecular phenotyping and functional assessment of smooth muscle like-cells with pathogenic variants in aneurysm genes ACTA2, MYH11, SMAD3 and FBN1. *Hum Mol Genet* 2021;**30**:2286–99.
37. van der Pluijm I, van Vliet N, von der Thusen JH. *et al.* Defective connective tissue Remodeling in Smad3 mice leads to accelerated aneurysmal growth through disturbed downstream TGF-beta Signaling. *EBioMedicine* 2016;**12**:280–94.
38. Huang S, Chen B, Humeres C. *et al.* The role of Smad2 and Smad3 in regulating homeostatic functions of fibroblasts in vitro and in adult mice. *Biochim Biophys Acta Mol Cell Res* 2020;**1867**:118703.
39. Bramel EE, Creamer TJ, Saqib M. *et al.* Postnatal Smad3 inactivation in murine smooth muscle cells elicits a temporally and regionally distinct transcriptional response. *Front Cardiovasc Med* 2022;**9**:826495.
40. Myung P, Andl T, Atit R. The origins of skin diversity: lessons from dermal fibroblasts. *Development* 2022;**149**:dev200298.
41. Pfaltzgraff ER, Shelton EL, Galindo CL. *et al.* Embryonic domains of the aorta derived from diverse origins exhibit distinct properties that converge into a common phenotype in the adult. *J Mol Cell Cardiol* 2014;**69**:88–96.
42. Cheung C, Bernardo AS, Trotter MW. *et al.* Generation of human vascular smooth muscle subtypes provides insight into embryological origin-dependent disease susceptibility. *Nat Biotechnol* 2012;**30**:165–73.
43. Zhang H, Gu S, Al-Sabeq B. *et al.* Origin-specific epigenetic program correlates with vascular bed-specific differences in Rgs5 expression. *FASEB J* 2012;**26**:181–91.
44. Haimovici H, Maier N. Experimental canine atherosclerosis in autogenous abdominal aortic grafts implanted into the jugular vein. *Atherosclerosis* 1971;**13**:375–84.
45. Lacolley P, Regnault V, Segers P. *et al.* Vascular smooth muscle cells and arterial stiffening: relevance in development, aging, and disease. *Physiol Rev* 2017;**97**:1555–617.
46. Owens GK, Kumar MS, Wamhoff BR. Molecular regulation of vascular smooth muscle cell differentiation in development and disease. *Physiol Rev* 2004;**84**:767–801.
47. Wang RN, Green J, Wang Z. *et al.* Bone morphogenetic protein (BMP) signaling in development and human diseases. *Genes Dis* 2014;**1**:87–105.

48. Oka T, Xu J, Molkentin JD. Re-employment of developmental transcription factors in adult heart disease. *Semin Cell Dev Biol* 2007;**18**:117–31.
49. Rajabi M, Kassiotis C, Razeghi P. *et al.* Return to the fetal gene program protects the stressed heart: a strong hypothesis. *Heart Fail Rev* 2007;**12**:331–43.
50. Uhlen M, Fagerberg L, Hallstrom BM. *et al.* Proteomics. Tissue-based map of the human proteome. *Science* 2015;**347**: 1260419.
51. Yeung KK, Bogunovic N, Keekstra N. *et al.* Transdifferentiation of human dermal fibroblasts to smooth muscle-like cells to study the effect of MYH11 and ACTA2 mutations in aortic aneurysms. *Hum Mutat* 2017;**38**:439–50.
52. Lowry OH, Rosebrough NJ, Farr AL. *et al.* Protein measurement with the Folin phenol reagent. *J Biol Chem* 1951;**193**: 265–75.
53. Schindelin J, Arganda-Carreras I, Frise E. *et al.* Fiji: an open-source platform for biological-image analysis. *Nat Methods* 2012;**9**:676–82.
54. Robinson JT, Thorvaldsdottir H, Winckler W. *et al.* Integrative genomics viewer. *Nat Biotechnol* 2011;**29**:24–6.
55. Chacko BM, Qin BY, Tiwari A. *et al.* Structural basis of heteromeric smad protein assembly in TGF-beta signaling. *Mol Cell* 2004;**15**:813–23.
56. *The PyMOL Molecular Graphics System, Version 1.8.* Schrödinger, LLC.
57. Aubart M, Gazal S, Arnaud P. *et al.* Association of modifiers and other genetic factors explain Marfan syndrome clinical variability. *Eur J Hum Genet* 2018;**26**:1759–72.
58. Campens L, Callewaert B, Muino Mosquera L. *et al.* Gene panel sequencing in heritable thoracic aortic disorders and related entities - results of comprehensive testing in a cohort of 264 patients. *Orphanet J Rare Dis* 2015;**10**:9.
59. Regalado ES, Guo DC, Villamizar C. *et al.* Exome sequencing identifies SMAD3 mutations as a cause of familial thoracic aortic aneurysm and dissection with intracranial and other arterial aneurysms. *Circ Res* 2011;**109**:680–6.
60. Velchev JD, Verstraeten A, Meester J. *et al.* Generation and validation of an iPSC line (BBANTWi008-A) from a Loeys-Dietz syndrome type 3 patient. *Stem Cell Res* 2022;**64**:102932.
61. Aubart M, Gobert D, Aubart-Cohen F. *et al.* Early-onset osteoarthritis, Charcot-Marie-tooth like neuropathy, autoimmune features, multiple arterial aneurysms and dissections: an unrecognized and life threatening condition. *PLoS One* 2014;**9**:e96387.
62. Abou Tayoun AN, Pesaran T, DiStefano MT. *et al.* Recommendations for interpreting the loss of function PVS1 ACMG/AMP variant criterion. *Hum Mutat* 2018;**39**:1517–24.
63. Cho YK, Won D-G, Keum C. *et al.* A novel PS4 criterion approach based on symptoms of rare diseases and in-house frequency data in a Bayesian framework. *BioRxiv*, july 2020.
64. Lek M, Karczewski KJ, Minikel EV. *et al.* Analysis of protein-coding genetic variation in 60,706 humans. *Nature* 2016;**536**:285–91.
65. Sian, Ellard ELB, Callaway A, Berry I. *et al. ACGS Best Practice Guidelines for Variant Classification in Rare Disease 2020*. Association for Clinical Genomic Science. https://www.acgs.uk.com/media/11631/uk-practice-guidelines-for-variant-classification-v4-01-2020.pdf2020.